Enhanced Activity for Electrocatalytic H_2 Production through Cooperative Pr and Bi Co-doping of CeO_2 in Solid Oxide Electrolysis Cells

Wu, Tiantian; Vegge, Tejs; Anton Hansen, Heine

Published in:
Journal of Catalysis

Link to article, DOI:
10.1016/j.jcat.2021.08.045

Publication date:
2021

Document Version
Peer reviewed version

Journal Pre-proofs

Enhanced Activity for Electrocatalytic H_2 Production through Cooperative Pr and Bi Co-doping of CeO_2 in Solid Oxide Electrolysis Cells

Tiantian Wu, Tejs Vegge, Heine Anton Hansen

PII: S0021-9517(21)00354-7
DOI: https://doi.org/10.1016/j.jcat.2021.08.045
Reference: YJCAT 14311

To appear in: *Journal of Catalysis*

Received Date: 9 June 2021
Revised Date: 2 August 2021
Accepted Date: 21 August 2021

Please cite this article as: T. Wu, T. Vegge, H. Anton Hansen, Enhanced Activity for Electrocatalytic H_2 Production through Cooperative Pr and Bi Co-doping of CeO_2 in Solid Oxide Electrolysis Cells, *Journal of Catalysis* (2021), doi: https://doi.org/10.1016/j.jcat.2021.08.045

Enhanced Activity for Electrocatalytic H_2 Production through Cooperative Pr and Bi Co-doping of CeO_2 in Solid Oxide Electrolysis Cells

Tiantian Wu, [a] Tejs Vegge, [a,*] Heine Anton Hansen [a,*]

[a] Department of Energy Conversion and Storage, Technical University of Denmark, Anker Engelunds Vej Building 301, 2800 Kgs. Lyngby, Denmark.

*Corresponding author:

Tejs Vegge E-mail: teve@dtu.dk

Heine Anton Hansen E-mail: heih@dtu.dk

Abstract

CeO_2-based catalysts as cathodes in solid oxide electrolysis cells (SOECs) have great potential for improving the storage of renewable electricity in the form of H_2 via the water-splitting reaction (WSR). A key challenge to promote the WSR on CeO_2 is facilitating the decomposition of stable surface hydroxides to form H_2. Here, we use density functional theory to investigate the effect of Bi- and Pr- doping for the WSR on CeO_2(111). We find that dopants influence the stability of hydridic H, which can be formed during the decomposition of hydroxyl to H_2. By stabilizing hydridic H on Bi during the H_2 formation step, Bi and Pr co-doped into ceria lower the barrier to H_2 formation, enhancing the rate of WSR by 2-4 orders of magnitude compared to individually Pr-, Bi- or Gd-doped CeO_2. We suggest co-doping as an effective strategy for improving the WSR in SOECs.

Keywords

DFT Studies, Hubbard Corrections, Reaction Mechanism, Metal-H Hydride Intermediates

1.Introduction

Ceria-based materials are good mixed ionic and electronic conductors exposing a large ceria-gas reaction interface and have thus been proposed as cathodes for the WSR in SOECs [1–5]. Investigations on water-associated reactions over ceria for H_2 production have demonstrated that the fundamental reaction steps of the WSR on CeO_2 include (a) the formation of oxygen vacancies (V_O), (b) water adsorption and dissociation into hydroxyls or hydridic H-species if the hydroxyl surface coverage is beyond one monolayer, and (c) hydroxyl or hydride decomposition into H_2 [1,4–9]. Among these, the decomposition into H_2 is the rate-determining step. Our previous studies have identified dramatically decreased reaction barriers for H_2 production via the formation of hydridic H-species on CeO_2 [4,5,7,9]. The facile formation of oxygen vacancies and hydroxyls on CeO_2 promotes over one monolayer H adsorption in the form of hydroxyl or hydridic H. Therefore, the key for improving the WSR is to stabilize the formation of reaction intermediates such as oxygen vacancies, hydroxyls and the hydridic H-species on CeO_2.

Our previous studies also demonstrated that the WSR activity of the (111) facet, the most stable terminations of CeO_2 [9,10], can be improved by stabilizing the formation of hydridic H-species by using strain engineering [5] or gadolinium doping [4]. Besides trivalent gadolinium doping, multivalent praseodymium (Pr^{3+}/Pr^{4+}) dopants are often used in CeO_2 due to their similar ionic radius to cerium and their good performance in improving the oxygen mobility and diminishing the reduction energy of CeO_2 [11,12]. It is suggested that a small addition of bismuth (Bi^{3+}/Bi^{5+}) in doped CeO_2 can further improve the ionic conductivity and maintain the phase stability while not significantly affecting the reduction energy of CeO_2 [13,14]. Therefore, encouraged by many successful applications of co-doping in enhancing the catalytic activity of CeO_2 [15–19], the size-matching between Pr and Ce, and the flexible +3/+5 oxidation numbers

of Bi, we here investigate the cooperative Pr and Bi co-doped CeO_2 for the WSR. In this work, we compare the WSR on Pr-doped, Bi-doped, Pr and Bi co-doped to stoichiometric CeO_2(111) by using density functional theory corrected for on-site Coulomb interactions (DFT+*U*). We systematically investigate the impact of Pr and Bi co-doping on the formation of V_O and hydroxyls (or hydridic H-species) on CeO_2 during the WSR and how the co-doping influences the reaction kinetics for H_2 formation.

2.Simulation Methods

The Pr and Bi co-doped CeO_2(111) is built as a 2×3 surface unit cell consisting of three O-Ce-O atomic layers [4] as presented in **Figure S1**, where a 15 Å vacuum gap is applied to block the interaction between periodic units. The O-Ce-O layer at the bottom is fixed during all DFT+*U* studies. The oxygen vacancy formation energy in the p(2×3) CeO_2(111) is 0.16 eV larger than using a larger p(3x4) unit cell [4]. We perform spin-polarized DFT calculations by using the Vienna ab initio simulation package (VASP) [20] with the Perdew-Burke-Ernzerhof (PBE) [21] functional. Spin polarization is considered with ferromagnetic ordering because of a small energy difference (<0.01 eV) between ferromagnetic and antiferromagnetic ordering [4]. VASP version 5.4.4 with POTCAR files version 5.2 is applied for all DFT calculations. A Hubbard *U* term (U_{eff}=4.5 eV [22–25]) is added to the PBE functional to improve the description of the electron localization on the 4f shells of both Ce and Pr. We expand wave functions in plane waves with an energy cutoff of 550 eV [4,5]. A *Γ*-centered 3×2×1 k-point mesh is used for sampling the Brillouin zone. The transition states (TS) and activation barriers are identified by the climbing image nudged-elastic band (NEB) method [26] as implemented in VASP, with a force tolerance of 0.03 eV /Å.

3.Results and discussions

We investigate different distributions of Pr and Bi in the co-doped CeO_2(111) and find that two substitutional dopants prefer to sit in the top layer as shown in **Figure S2**, where Pr^{3+} and Bi^{5+} are observed in **Figure S3**. After creating one V_O, Pr^{3+} and Bi^{3+} are identified as the most stable states in **Figures S4** and **S5**. **Figure 1** shows that the formation energy of a single oxygen vacancy (V_O) in the doped CeO_2 is 1.5 eV lower than in the stoichiometric CeO_2(111). Therefore, the Pr and Bi co-doping is excellent at stabilizing V_O formation, especially in the top surface (V_O^{sur}) as shown in **Figure 1**.

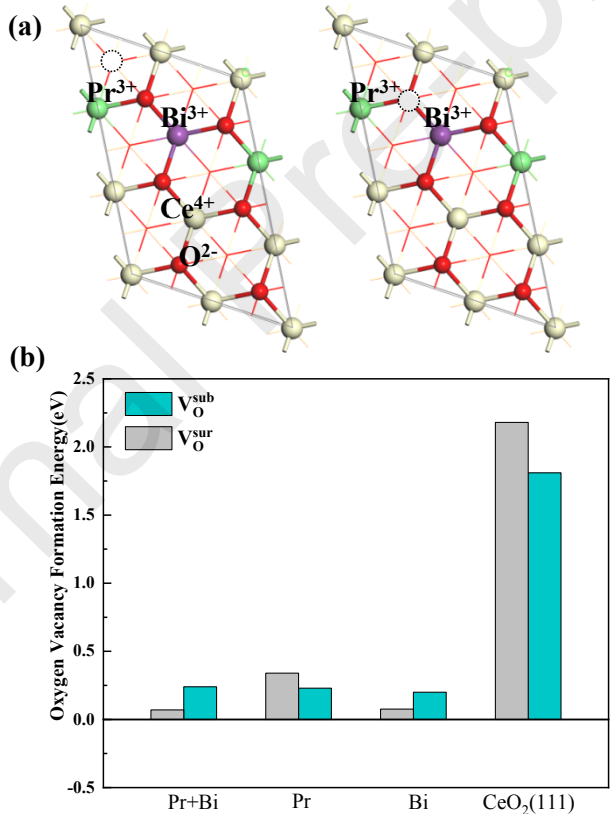

Figure 1. (a) Configurations of one V_O (dashed ball) in the subsurface (V_O^{sub}) and top surface (V_O^{sur}) of the Pr and Bi co-doped CeO_2(111). The atoms in the deep layers are displayed as lines. (b) The formation energy of one V_O in doped and stoichiometric CeO_2(111).

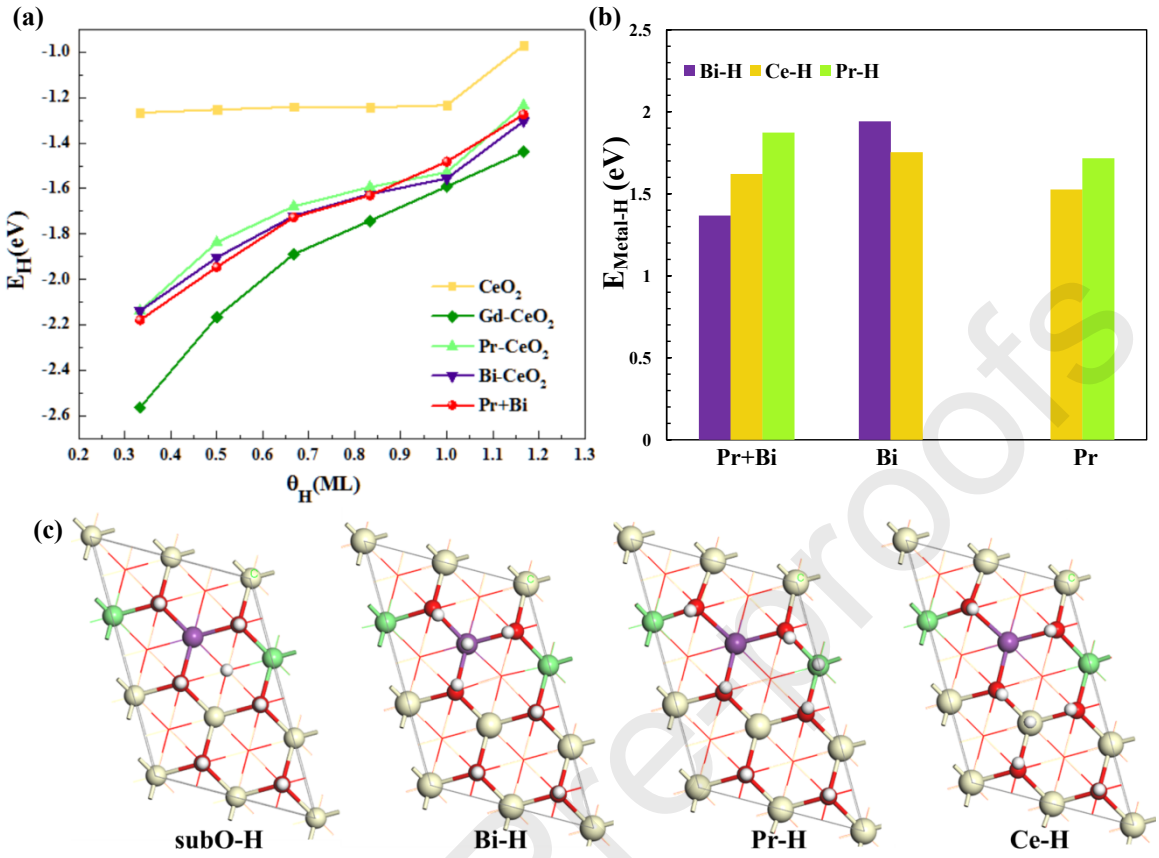

Figure 2. (a) The average hydrogen adsorption energy (E_H) on the doped and stoichiometric CeO_2(111) as a function of hydrogen coverage Θ_H (in monolayers, ML). (b) The formation energy of Metal-H hydrides ($E_{Metal-H}$, the differential E_H at Θ_H =1.17 ML) on the doped CeO_2. (c) The configurations of 7H adsorption on the Pr and Bi co-doped CeO_2(111): H binds to a lattice oxygen in the subsurface (subO-H); H binds to Bi (Bi-H), Pr (Pr-H) or Ce (Ce-H) in the top surface.

In addition to the facile formation of V_O in doped CeO_2, the hydrogen adsorption via water dissociation on doped ceria also becomes more favorable than on stoichiometric ceria as presented in **Figure 2**, where we find a much lower hydrogen adsorption energy (E_H) on doped ceria at different hydrogen coverage Θ_H ($\Theta_H = N_H/N$, N_H is the number of the adsorbed H while

N is the total number of the exposed lattice oxygen of ceria, and N=6 in our studied surfaces). All possible configurations of hydrogen at different coverage on co-doped ceria are presented in **Figures S6** and **S7**, showing higher preference for hydrogen adsorption near Pr+Bi pairs than near Ce. **Figure 2(a)** shows a similar trend of the average E_H on Pr-doped, Bi-doped and Pr+Bi co-doped ceria, and also a small E_H difference between them arising from the similar ionic radius among Pr, Bi and their Pr+Bi pairs (as shown in **Table S1**) and correspondingly similar H binding. However, when Θ_H increases above 1 ML (7H), we note the differential E_H on co-doped ceria is at least 0.2 eV lower than that on Pr- or Bi-doped ceria from **Figure S8**, indicating Pr+Bi co-doping facilitates the formation of 7H. For the high coverage regime with adsorption of 7 hydrogen (7H, Θ_H =1.17 ML) on the Pr and Bi co-doped ceria, we have identified four stable configurations as shown in **Figure 2**, including hydridic H-species (Metal-H hydrides) such as Bi-H, Pr-H and Ce-H. Although it is not as facile as previously reported on Gd doped ceria [4], the formation of 7H on the Pr and Bi co-doped ceria is 0.2 and 0.5 eV respectively more stable than the Bi- and Pr-doped ceria as presented in **Figure S8**, which indicates that the cooperative effect of Pr and Bi co-doping effectively improves the stability of hydroxylated ceria at Θ_H =1.17 ML. Besides, from **Figure 2(b)** we can observe a much more stable hydridic H-species (Bi-H) on the co-doped CeO_2(111) compared to the Bi-doped and Pr-doped CeO_2(111). Bi-H becomes more stable than Ce-H on the co-doped system, while the formation of Ce-H is preferred over Bi-H (or Pr-H) in the single doped system. Therefore, the stability of the hydridic H-species on ceria is significantly improved by the Pr and Bi co-doping. **Figure S9** shows the energy difference of E_H between the ceria slab with 3 and 4 O-Ce-O layers is within 0.01 eV, indicating the proper accuracy of E_H calculated by using our simulation models.

In addition, we have tested the effect of the U_{eff} value on the relative stability of Bi-H, Ce-H and Pr-H on individually doped and co-doped ceria surfaces as shown in **Figures S10** and **S11**. **Figure S10** shows that the formation energy of hydridic H-species becomes more positive with increasing U_{eff}, agreeing well with previous findings that Hubbard corrections cause adsorption energies to be more endothermic [4,27]. Additionally, the formation energy of Bi-H on the co-doped ceria remains at the lowest level under different U_{eff} in **Figure S11**, showing that the favorable formation of Bi-H on the co-doped ceria is not affected by the exact U_{eff} value.

Then, we calculate the free energies of the reaction intermediates on the doped CeO_2 relative to their clean surfaces by using a DFT-based thermodynamics method described in our previous work [4,5,7]. Accordingly, the ceria-gas interface is assumed in equilibrium with water steam and hydrogen molecules at 1 bar partial pressure, and reaction intermediates form via reactions between oxygen vacancies and water at the clean surface. The free energy diagrams and the illustrated reaction steps during the WSR over the doped CeO_2 at 800 K are given in **Figures 3(a)** and **S12-S16**. The hydroxyl decomposition into H_2 is the rate-determining step for the WSR on Pr+Bi co-doped ceria, similar to our findings on Gd-doped and strained ceria [4,5,7]. The breaking of the first O-H bond in the H_2 production step is difficult, and the TS is associated with this bond breaking as shown in NEB paths in **Figures S17-S31**. **Figures S17-S31** also include details of the structural and electronic changes during the H_2 production step. Because of the high reaction barrier for hydroxyl decomposition into H_2 on the 2H covered surface, it is more favorable to form another V_O on the 2H surface than producing H_2 directly via 2H, as shown in **Figure S12**. The barrier for H_2 formation via $2H+V_O$ exceeds 3.0 eV, leading to additional water adsorption and dissociation into 4H, 5H, 6H, and 7H on the co-doped CeO_2. **Figure 3(a)** gives simplified free energy diagrams for these dominant WSR pathways through 6H, Bi-H, Ce-H, or

Pr-H intermediates at 800 K. For the 6H surface, all surface O is reduced to hydroxyl, and H_2 can be formed by decomposition of this hydroxyl through a 2.9 eV barrier. The 7H surface is most stable when the excess H atom is in the subsurface as hydroxyl (subO-H). The 7H surface decomposes most easily to H_2, however, through the formation of an Metal-H hydride intermediate. The stability of the hydridic H-species on the co-doped CeO_2 in **Figure 3(a)** follows the order of Bi-H > Ce-H > Pr-H. Besides, a lower reaction barrier is required for producing H_2 via Bi-H than Ce-H and Pr-H as shown in **Figure 3(a)**, leading to substantially enhanced WSR activity via the Bi-H pathway. The structural and electronic changes during the reactions to produce H_2 via 7H→TS→(Bi/Pr/Ce)H→5H+H_2 are presented in **Figure S18**, where $Bi^{3+}H^-$, $Pr^{3+}H^-$ and $Ce^{4+}H^-$ hydridic H-species are identified based on magnetic moments. In comparison, Ce-H is more stable than Bi-H in the Bi-doped CeO_2, leading to H_2 production via the Ce-H pathway as shown in **Figure S16**. Because Ce-H is more easily formed than Pr-H on Pr-doped ceria, the fastest reaction pathway on Pr-doped ceria proceeds via Ce-H formation of as shown in **Figure S15.** Therefore, the fastest reaction pathway for the WSR on ceria shifts from Ce-H to Bi-H by the cooperative effect of Pr and Bi co-doping because of the more favorable formation of Bi-H over Ce-H on the co-doped ceria. In addition, we have compared reaction pathways of the WSR (at 800 K) on the Pr and Bi co-doped CeO_2(111) with Pr and Bi sitting in the different atomic layers as shown in **Figure S32**, where Pr and Bi both sit in the top surface shows the best activity for the WSR because of the more facile formation of the reaction intermediates such as oxygen vacancies, hydroxyls and hydridic H-species. In all cases, the trend in the TS energy of the 7H→TS→Metal-H step follows the trend in Metal-H final state energy, which suggests the stability of the Metal-H hydride can be important to enhance the rate of H_2 formation.

As we have done in previous studies [5,9], the activity of doped and un-doped ceria surfaces for the WSR is evaluated by calculating the turnover frequency (TOF) based on the energetic span model [28,29]. In **Figure 3(a)**, the $5H+V_O^{sur}$ marked in purple is the most stable reaction intermediate and thus is the TOF-determining intermediate (TDI), while the TS for the H_2 production via the Bi-H is the lowest and thus is the TOF-determining TS (TDTS). The energy difference between the TDI and the TDTS is the required free energy for the WSR on the Pr and Bi co-doped ceria, which is used for calculating the TOF. **Figure 3(b)** shows that the TOF for the WSR on doped ceria is larger than the clean CeO_2. In addition, we observe a significantly increased TOF for the Pr and Bi co-doped ceria compared to Bi-doped and Pr-doped CeO_2 as well as Gd-doped [4] CeO_2, suggesting that Pr and Bi co-doping effectively improves the activity of CeO_2 for H_2 production. Finally, we test the sensitivity of our findings to the reaction gas composition, by calculating TOF for WSR over ceria in SOECs in an operating environment, which is under an $50\%H_2O$-$50\%H_2$ atmosphere [30,31] and at intermediate temperature below 1000 K [32,33]. As shown in **Figure S33**, the Pr and Bi co-doped ceria holds the best activity toward H_2 production compared to the other doped ceria and clean ceria surface at T<900 K under $50\%H_2O$-$50\%H_2$, while the activity of the co-doped ceria becomes close to the Pr doped ceria at T>900 K. Under an extreme $90\%H_2O$-$10\%H_2$ atmosphere, Pr and Bi co-doped ceria still has the highest TOF for WSR at temperature below 1000 K, compared to the individually doped ceria as shown in **Figure S34**. Therefore, our DFT calculations predict that the Pr and Bi co-doped CeO_2 can hold excellent performance for the WSR at low and intermediate temperatures (below 900 K), arising from the improved stability of the hydridic H-species by Pr and Bi co-doping. In addition to the facile formation of oxygen vacancies, hydroxyls and hydridic H-species in the co-doped CeO_2, we find that the doping energy [34] of the Pr and Bi co-doped

CeO_2 is comparable to the Pr-doped CeO_2 as listed in **Table S1**, indicating the relatively facile addition of Bi into the Pr doped CeO_2. **Table S1** further shows that Pr and Bi dopants are energetically preferred at the surface of ceria rather than in the bulk.

By performing DFT+*U* studies on the Pr-doped, Bi-doped, and Pr and Bi co-doped ceria for WSR, we find the stability of reaction intermediates such as V_O, hydroxyls and especially the hydridic H-species during the WSR on ceria is substantially improved by Pr and Bi co-doping, leading to significantly enhanced performance for the H_2 production by the co-doping. Our studies suggest a wide application of cooperative co-doping in enhancing the activity of ceria for the WSR in SOECs, due to the induced change in the reaction pathways though the hydridic co-dopant-H (e.g. Bi-H) intermediate.

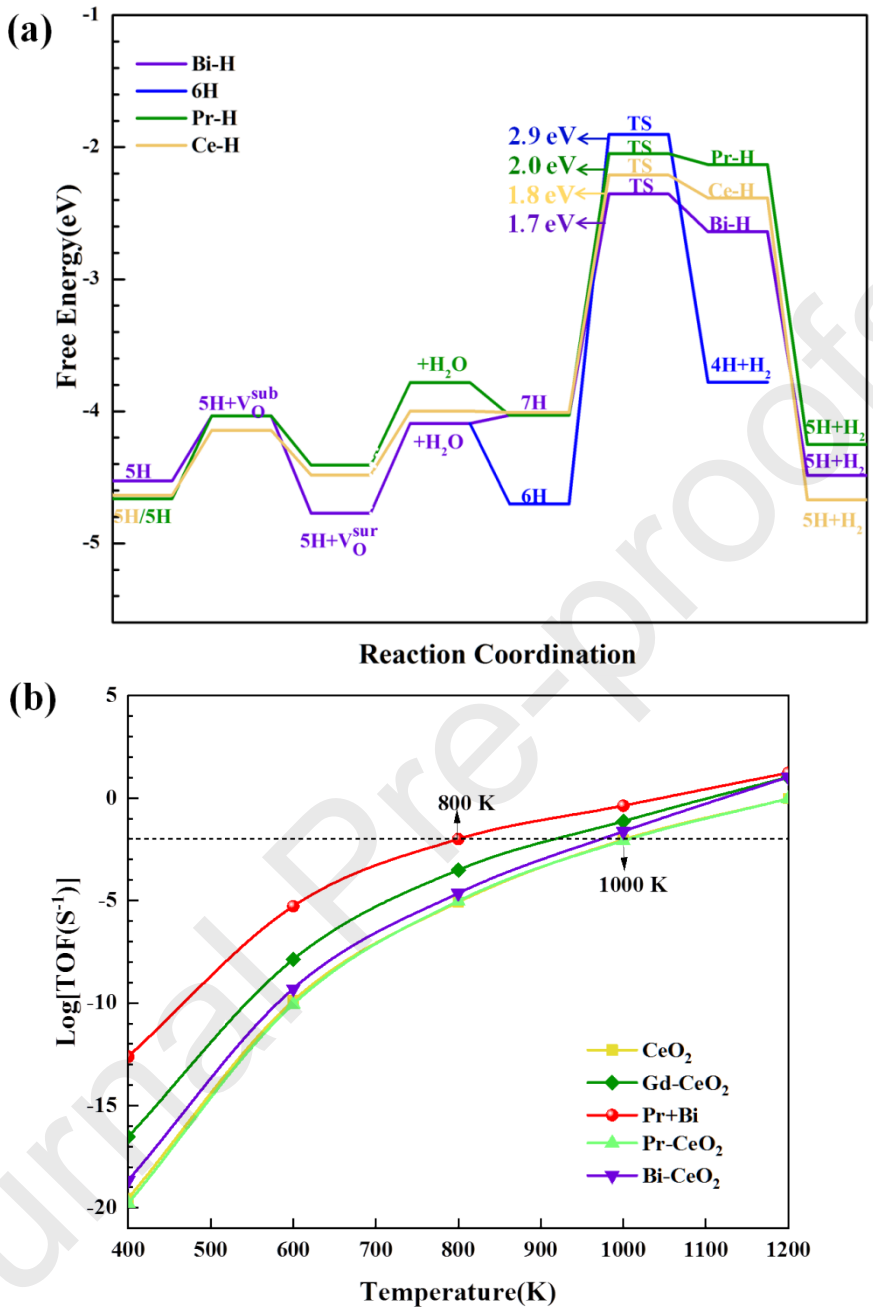

Figure 3. (a) Dominant reaction pathways of the WSR on the Pr and Bi co-doped CeO_2(111) via the formation of 6H, Bi-H, Ce-H or Pr-H at 800 K and 1 bar partial pressure. The NEB paths for the formation of Pr-H, Ce-H or Bi-H are given in **Figure S17** and related configurations of each

reaction intermediates are presented in **Figure S18.** (b) The TOF of the WSR on the doped and stoichiometric CeO_2(111) as a function of operating temperature.

Supporting Information

Supporting figures with free energy diagrams of reaction pathways, atomic configurations during WSR pathways, NEB paths at H_2 production step, tests on effect of different U_{eff}, TOF in a 50%H_2O-50%H_2 and a 90%H_2O-10%H_2 atmosphere at 1 bar total pressure, and a supporting table of doping energy.

Acknowledgements

This work was financially supported by the VILLUM FONDEN through the research center V-Sustain (grant number 9455).

References

[1] Z.A. Feng, F. El Gabaly, X. Ye, Z.-X. Shen, W.C. Chueh, Fast vacancy-mediated oxygen ion incorporation across the ceria–gas electrochemical interface, Nat. Commun. 5 (2014) 4374.

[2] J.T.S. Irvine, D. Neagu, M.C. Verbraeken, C. Chatzichristodoulou, C. Graves, M.B. Mogensen, Evolution of the electrochemical interface in high-temperature fuel cells and electrolysers, Nat. Energy. 1 (2016) 15014.

[3] F.M. Sapountzi, J.M. Gracia, C.J. Weststrate, H.O.A. Fredriksson, J.W. Niemantsverdriet, Electrocatalysts for the generation of hydrogen, oxygen and synthesis gas, Prog. Energy Combust. Sci. 58 (2017) 1–35.

[4] T. Wu, Q. Deng, H.A. Hansen, T. Vegge, Mechanism of water splitting on gadolinium-doped CeO_2(111): A DFT+U study, J. Phys. Chem. C. 123 (2019) 5507–5517.

[5] T. Wu, T. Vegge, H.A. Hansen, Improved electrocatalytic water splitting reaction on CeO_2(111) by strain engineering: A DFT+U study, ACS Catal. 9 (2019) 4853–4861.

[6] M. Molinari, S.C. Parker, D.C. Sayle, M.S. Islam, Water adsorption and its effect on the stability of low index stoichiometric and reduced surfaces of ceria, J. Phys. Chem. C. 116 (2012) 7073–7082.

[7] H.A. Hansen, C. Wolverton, Kinetics and thermodynamics of H_2O dissociation on reduced CeO_2(111), J. Phys. Chem. C. 118 (2014) 27402–27414.

[8] Z. Yang, Q. Wang, S. Wei, D. Ma, Q. Sun, The Effect of environment on the reaction of water on the ceria (111) surface: A DFT+*U* study, J. Phys. Chem. C. 114 (2010) 14891–14899.

[9] T. Wu, N. López, T. Vegge, H.A. Hansen, Facet-dependent electrocatalytic water splitting reaction on CeO_2: A DFT+*U* study, J. Catal. 388 (2020) 1–10.

[10] Y. Jiang, J.B. Adams, M. Van Schilfgaarde, Density-functional calculation of CeO_2 surfaces and prediction of effects of oxygen partial pressure and temperature on stabilities, J. Chem. Phys. 123 (2005) 064701.

[11] K. Ahn, D.S. Yoo, D.H. Prasad, H.-W. Lee, Y. Chung, J.-H. Lee, Role of multivalent Pr in the formation and migration of oxygen vacancy in Pr-doped Ceria: Experimental and first-principles investigations, Chem. Mater. 24 (2012) 4261–4267.

[12] P.P. Dholabhai, J.B. Adams, P. Crozier, R. Sharma, Oxygen vacancy migration in ceria and Pr-doped ceria: A DFT+*U* study, J. Chem. Phys. 132 (2010) 094104.

[13] S. Dikmen, H. Aslanbay, E. Dikmen, O. Şahin, Hydrothermal preparation and electrochemical properties of Gd^{3+}, Sm^{3+}, La^{3+}, and Nd^{3+} codoped ceria-based electrolytes for intermediate temperature-solid oxide fuel cell, J. Power Sources. 195 (2010) 2488–2495.

[14] G. Accardo, L. Spiridigliozzi, G. Dell'Agli, S.P. Yoon, D. Frattini, Morphology and structural stability of bismuth-gadolinium co-doped ceria electrolyte nanopowders, Inorganics. 7 (2019) 1–10.

[15] Y. Park, S.K. Kim, D. Pradhan, Y. Sohn, Surface treatment effects on CO oxidation reactions over Co, Cu, and Ni-doped and codoped CeO_2 catalysts, Chem. Eng. J. 250 (2014) 25–34.

[16] Z. Pu, X. Liu, A. Jia, Y. Xie, J. Lu, M. Luo, Enhanced activity for CO oxidation over Pr- and Cu-doped CeO_2 catalysts: Effect of oxygen vacancies, J. Phys. Chem. C. 112 (2008) 15045–15051.

[17] S. Banerjee, P.S. Devi, D. Topwal, S. Mandal, Enhanced ionic conductivity in $Ce_{0.8}Sm_{0.2}O_{1.9}$: Unique effect of calcium co-doping, Adv. Funct. Mater. 17 (2007) 2847–2854.

[18] Y. Dong, S. Hampshire, B. Lin, Y. Ling, X. Zhang, High sintering activity Cu–Gd co-doped CeO_2 electrolyte for solid oxide fuel cells, J. Power Sources. 195 (2010) 6510–6515.

[19] G. Zhou, W. Xiao, W. Geng, J. Wang, B. Xue, L. Wang, Improvement of the homogeneity and oxygen storage capability of Ce_{1-x} $Zr_xO_{2-\delta}$ by co-doping: A first-principles study, J. Alloys Compd. 817 (2020) 153238.

[20] G. Kresse, J. Furthmüller, Efficient iterative schemes for ab initio total-energy calculations using a plane-wave basis set, Phys. Rev. B. 54 (1996) 11169–11186.

[21] J.P. Perdew, K. Burke, M. Ernzerhof, Generalized gradient approximation made simple, Phys. Rev. Lett. 77 (1996) 3865–3868.

[22] M. Capdevila-Cortada, M. García-Melchor, N. López, Unraveling the structure sensitivity in methanol conversion on CeO_2: A DFT+U study, J. Catal. 327 (2015) 58–64.

[23] Y.-Q. Su, I.A.W. Filot, J.X. Liu, I. Tranca, E.J.M. Hensen, Charge transport over the defective CeO_2(111) surface, Chem. Mater. 28 (2016) 5652–5658.

[24] S. Fabris, S.D. Gironcoli, S. Baroni, G. Vicario, G. Balducci, Reply to “comment on 'taming multiple valency with density functionals: A case study of defective ceria'”, Phys. Rev. B. 72 (2005) 237102.

[25] K. Michel, T.S. Bjørheim, T. Norby, J. Janek, M.T. Elm, Importance of the spin-orbit interaction for a consistent theoretical description of small polarons in Pr-doped CeO_2, J. Phys. Chem. C. 124 (2020) 15831–15838.

[26] G. Henkelman, B.P. Uberuaga, H. Jónsson, Climbing image nudged elastic band method for finding saddle points and minimum energy paths, J. Chem. Phys. 113 (2000) 9901–9904.

[27] Z. Xu, J. Rossmeisl, J.R. Kitchin, A linear response DFT+*U* study of trends in the oxygen evolution activity of transition metal rutile dioxides, J. Phys. Chem. C. 119 (2015) 4827–4833.

[28] S. Kozuch, A refinement of everyday thinking: The energetic span model for kinetic assessment of catalytic cycles, WIREs Comput. Mol. Sci. 2 (2012) 795–815.

[29] S. Kozuch, S. Shaik, How to conceptualize catalytic cycles? the energetic Span model, Acc. Chem. Res. 44 (2011) 101–110.

[30] X. Tong, S. Ovtar, K. Brodersen, P.V. Hendriksen, M. Chen, A 4×4 cm^2 nanoengineered solid oxide electrolysis cell for efficient and durable hydrogen production, ACS Appl. Mater. Interfaces. 11 (2019) 25996–26004.

[31] S. Koch, P. V. Hendriksen, M. Mogensen, Y.-L. Liu, N. Dekker, B. Rietveld, B. De Haart, F. Tietz, Solid oxide fuel cell performance under severe operating conditions, Fuel Cells. 6 (2006) 130–136.

[32] W. Jung, J.O. Dereux, W.C. Chueh, Y. Hao, S.M. Haile, High electrode activity of nanostructured, columnar ceria films for solid oxide fuel cells, Energy Environ. Sci. 5 (2012) 8682–8689.

[33] W.C. Chueh, Y. Hao, W. Jung, S.M. Haile, High electrochemical activity of the oxide phase in model ceria-Pt and ceria-Ni composite anodes, Nat. Mater. 11 (2012) 155–161.

[34] A.K. Lucid, P.R.L. Keating, J.P. Allen, G.W. Watson, Structure and reducibility of CeO_2 doped with trivalent cations, J. Phys. Chem. C. 120 (2016) 23430–23440.

Declaration of interests

☒ The authors declare that they have no known competing financial interests or personal relationships that could have appeared to influence the work reported in this paper.

☐The authors declare the following financial interests/personal relationships which may be considered as potential competing interests:

- DFT is used to study water-splitting reaction on Pr and Bi co-doped ceria.
- The stabilized hydridic H on Bi by co-doping lowers the barrier to H_2 formation.
- The activity for H_2 formation on ceria is enhanced by Pr and Bi co-doping.
- The improved stability of Bi-H by co-doping contributes to the enhanced activity.